Supporting Information

Structural Disproportionation of $Ag_{20}Cu_{10}$ Highlights the Impact of Cluster Structure on Electrocatalytic Properties for CO_2 reduction

Yujiao Wang,[≠,a] Lin Xiong,[≠,b] Qian Cheng,[a] Daqiao Hu,[a] Shan Jin,*[,a] and Manzhou Zhu [a]

a. Key Laboratory of Structure and Functional Regulation of Hybrid Materials, Anhui University, Ministry of Education, Institutes of Physical Science and Information Technology, Anhui University, Department of Chemistry and Center for Atomic Engineering of Advanced Materials, Anhui University, Anhui 230601, P. R. China

b. School of Food and Chemical Engineering, Shaoyang University, Shaoyang 422000, P. R. China

≠ These authors contributed equally to this work.

Email: hudaqiao@ahu.edu.cn; jinshan@ahu.edu.cn

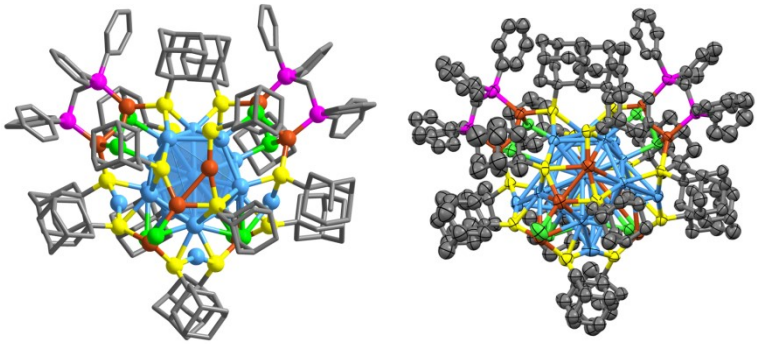

Figure S1. The overall structure and the ORTEP drawing (50% probability) of $Ag_{20}Cu_{10}(Dppm)_2(SAdm)_{14}Cl_8$. Atom colours: Cu = brown, S= yellow, P = purple, Cl = green; C = grey. H atoms are omitted.

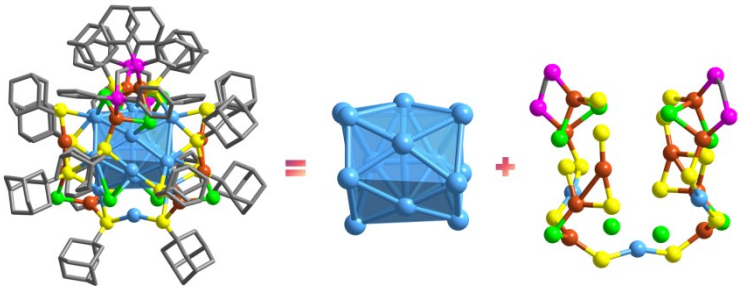

Figure S2. The framework of $Ag_{20}Cu_{10}(Dppm)_2(SAdm)_{14}Cl_8$ consisting of a Ag_{17} core and the big peripheral motif and two terminal Cl ligands.

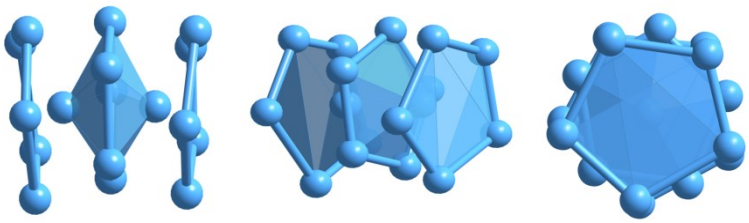

Figure S3. The Ag_{17} core can be regarded as a decahedral Ag_7 unit, with each side protected by an Ag_5 face.

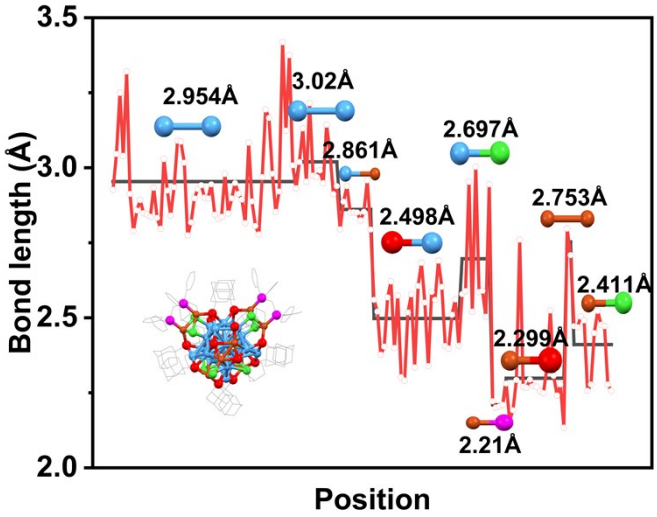

Figure S4. The bond lengths of the $Ag_{20}Cu_{10}(Dppm)_2(SAdm)_{14}Cl_8$ clusters.

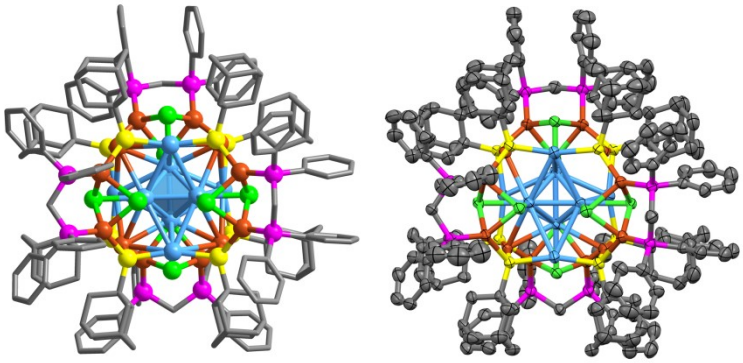

Figure S5. The overall structure and the ORTEP drawing (50% probability) of $[Ag_8Cu_{12}(Dppm)_4(SAdm)_8Cl_8]^{2+}$. Atom colours: Cu = brown, S= yellow, P = purple, Cl = green; C = grey. H atoms are omitted.

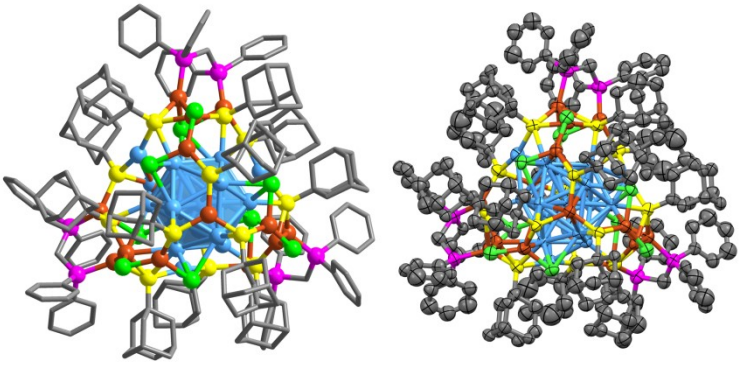

Figure S6. The overall structure and the ORTEP drawing (50% probability) of $[Ag_{17}Cu_{15}(SAdm)_{13}(Dppm)_3Cl_9]^{2+}$. Atom colours: Cu = brown, S= yellow, P = purple, Cl = green; C = grey. H atoms are omitted.

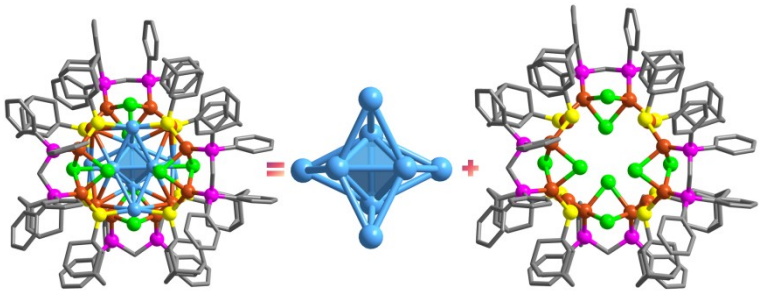

Figure S7. The $[Ag_8Cu_{12}(Dppm)_4(SAdm)_8Cl_8]^{2+}$ consists of a Ag_8 structure, surrounding by a complex shell.

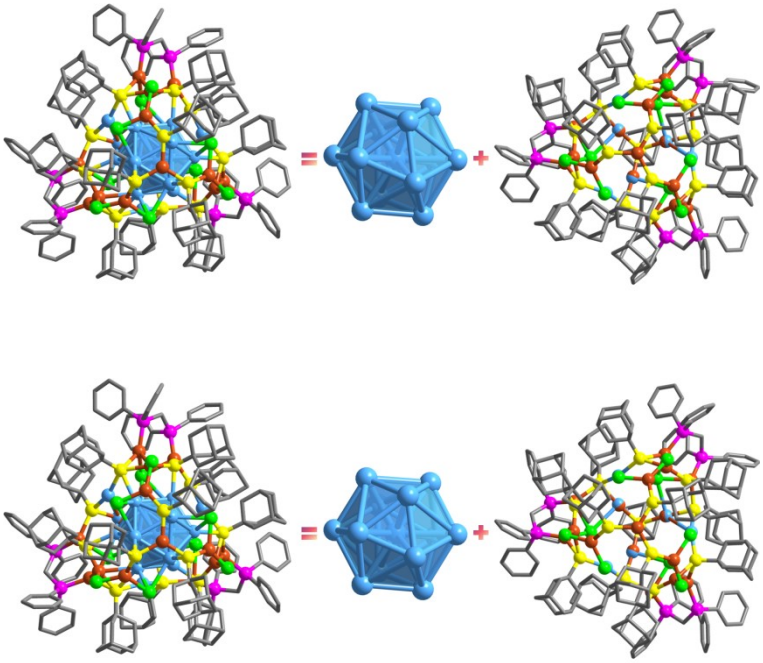

Figure S8. The $[Ag_{17}Cu_{15}(SAdm)_{13}(Dppm)_3Cl_9]^{2+}$ consists of a icosahedral Ag_{13} core, surrounding by a complex shell.

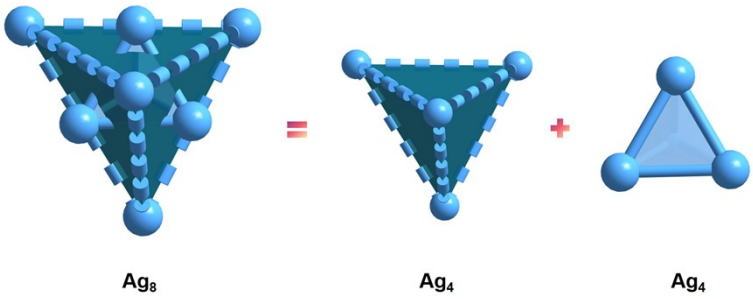

Figure S9. The Ag_8 structure in Ag_8Cu_{12} can be regarded as a combination of two Ag_4 tetrahedrons.

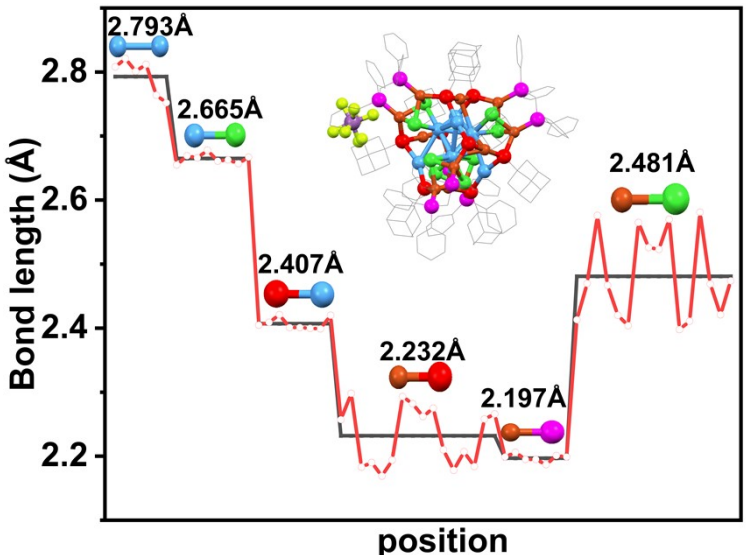

Figure S10. The bond lengths of the $Ag_8Cu_{12}(Dppm)_4(SAdm)_8Cl_8$ clusters.

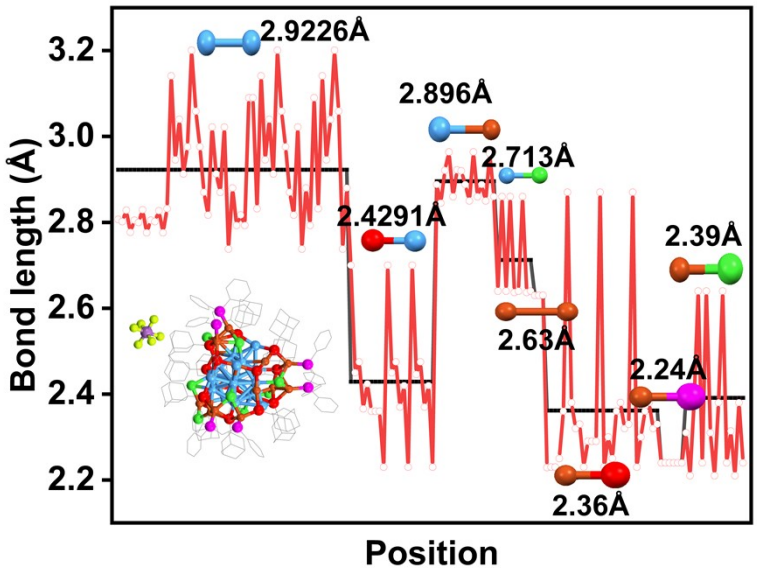

Figure S11. The bond lengths of the $Ag_{17}Cu_{15}(Dppm)_3(SAdm)_{13}Cl_9$ clusters.

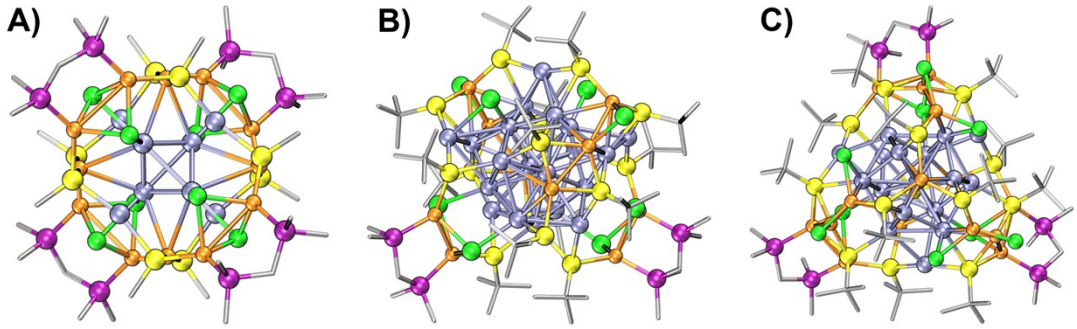

Figure S12. Energy minimum structures of $\mathbf{Ag_8Cu_{12}}$ (a), $\mathbf{Ag_{20}Cu_{10}}$ (b) and $\mathbf{Ag_{17}Cu_{15}}$ (c) after geometric optimization.

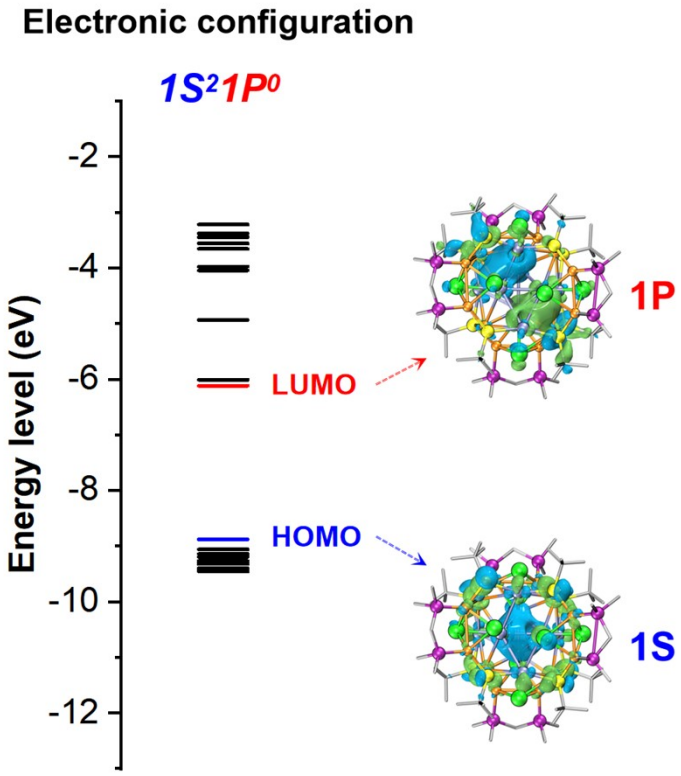

Figure S13. Kohn-sham molecular orbital energy level diagram of Ag_8Cu_{12}. As an illustration, only the isosurface diagrams of two frontier MOs (HOMO and LUMO) are shown here, with an isosurface value of 0.02.

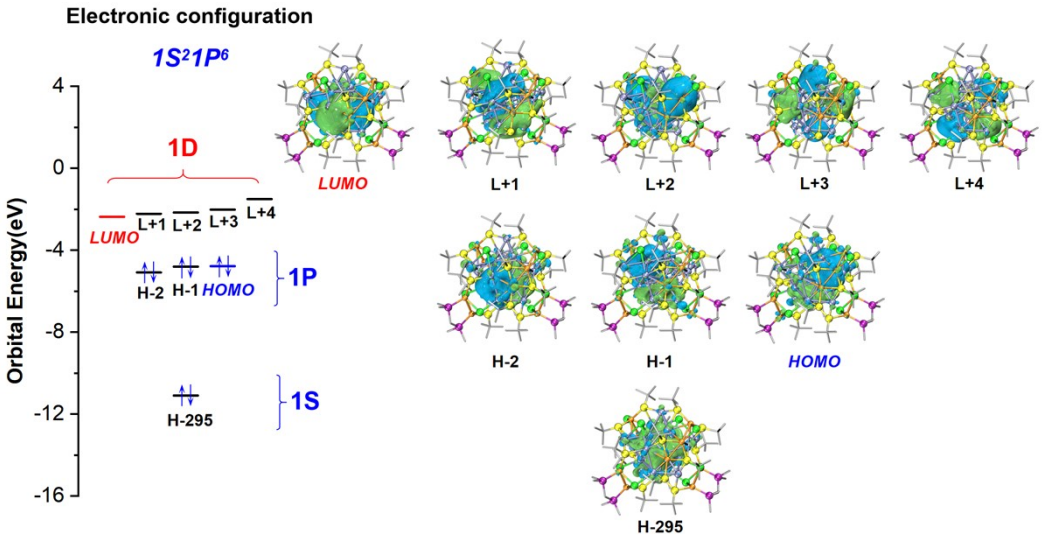

Figure S14. Kohn-sham molecular orbital energy level diagram of $Ag_{20}Cu_{10}$, with an isosurface value of 0.02.

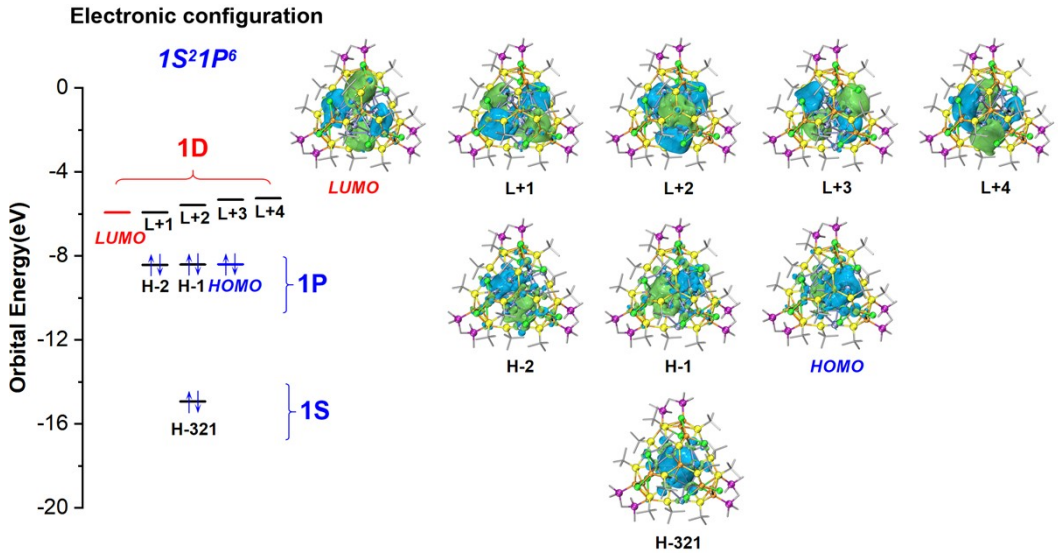

Figure S15. Kohn-sham molecular orbital energy level diagram of $Ag_{17}Cu_{15}$, with an isosurface value of 0.02.

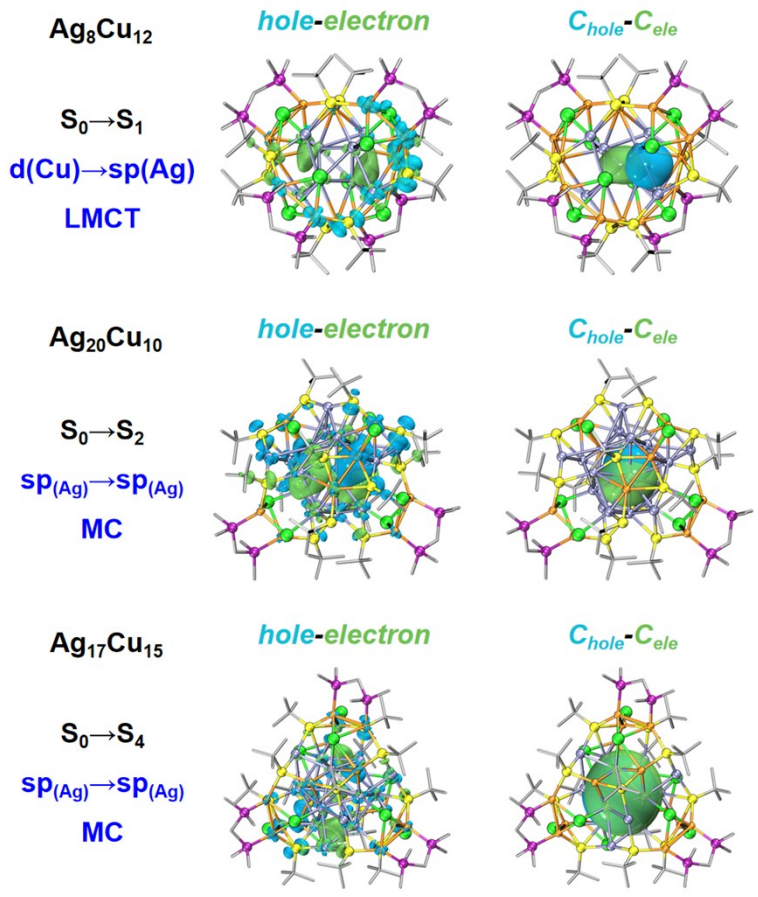

Figure S16. The hole-electron distribution of the lowest excited state allowed by transitions for Ag_8Cu_{12}, $Ag_{20}Cu_{10}$ and $Ag_{17}Cu_{15}$ clusters. The green and cyan isosurfaces represent the distribution of electrons and holes, respectively. The value of the hole-electron isosurface is 0.002, and the value of the Chole and Cele isosurface is 0.0005.

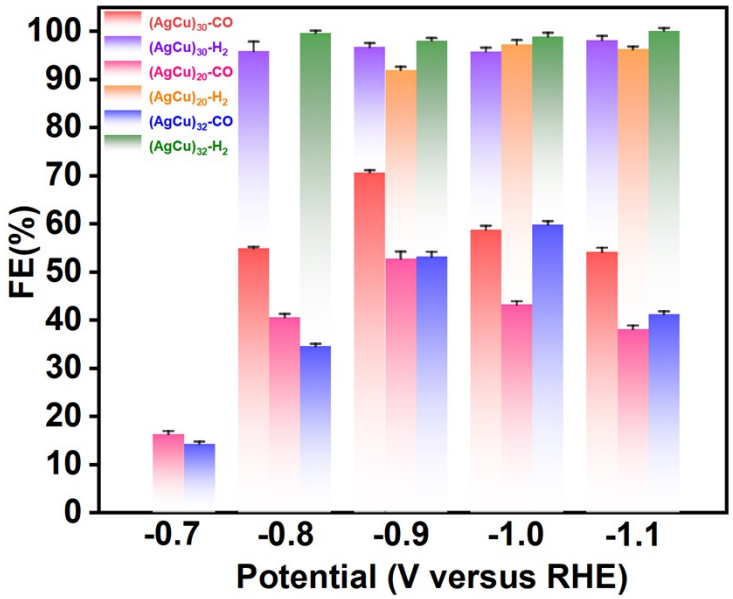

Figure S17. The Faradaic efficiency for the CO_2 reduction products of the series of Ag-Cu alloy nanoclusters.

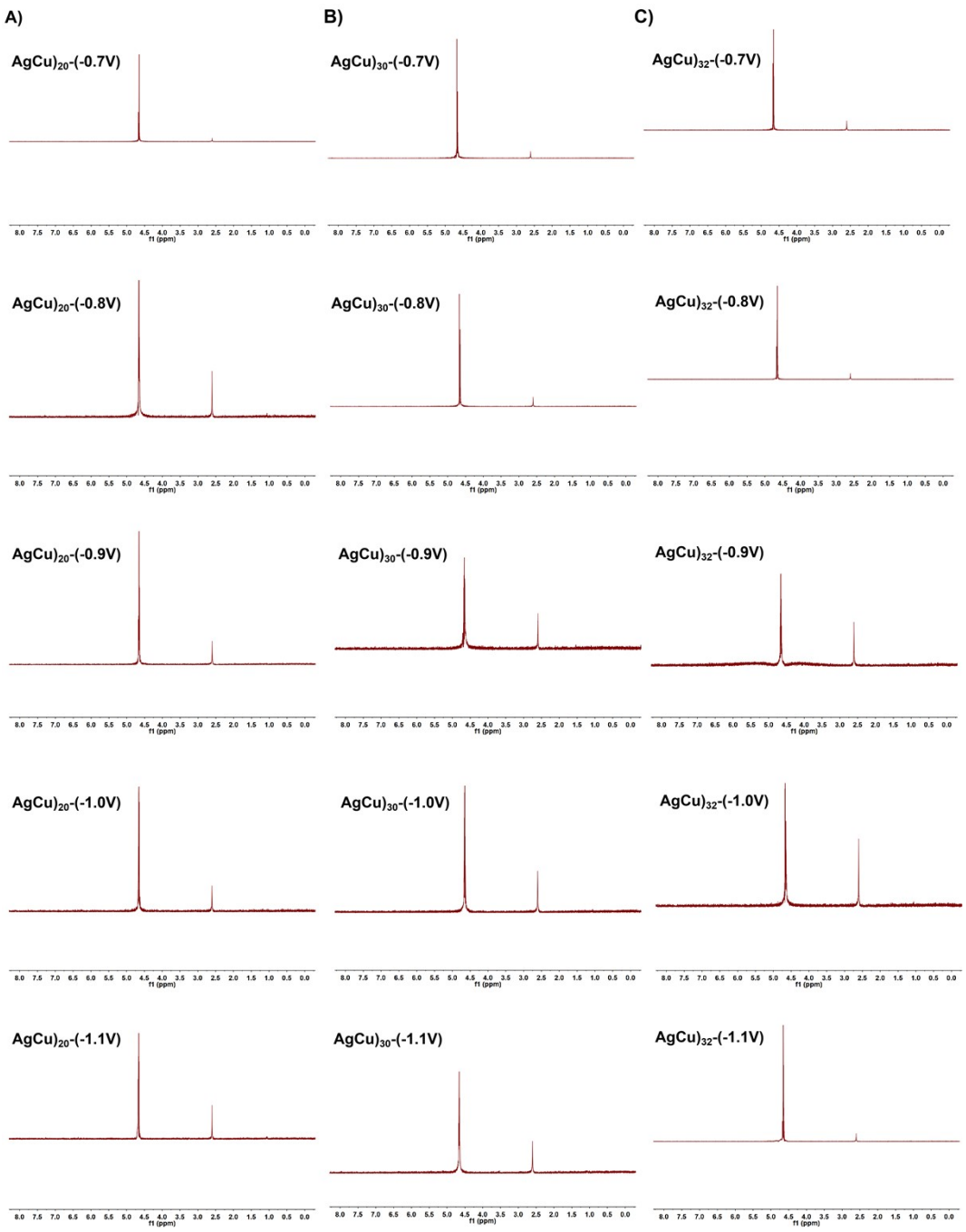

Figure S18. HNMR spectra of electrolyte after 10 minutes of electrocatalytic CO_2 reduction, with deuterated D_2O as the deuterated solvent and deuterated DMSO as the internal standard.

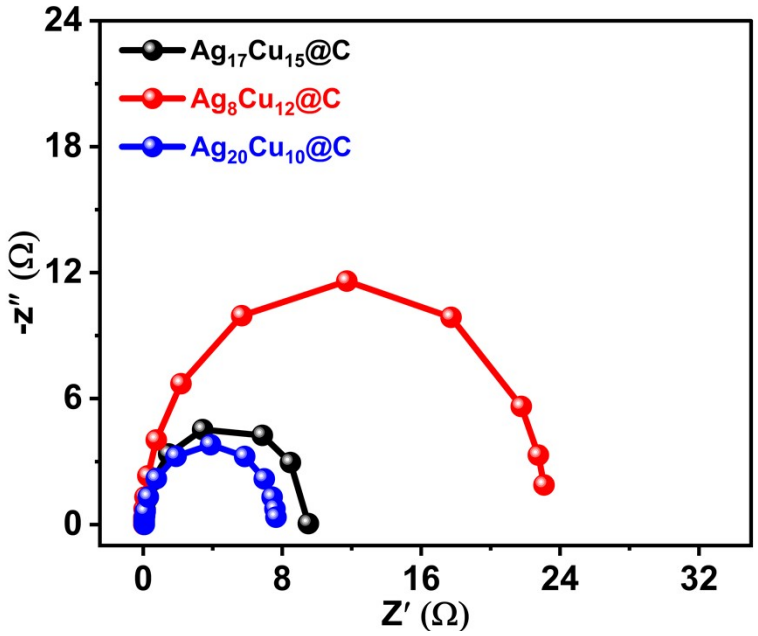

Figure S19. The EIS of three nanoclsuters catalyst.

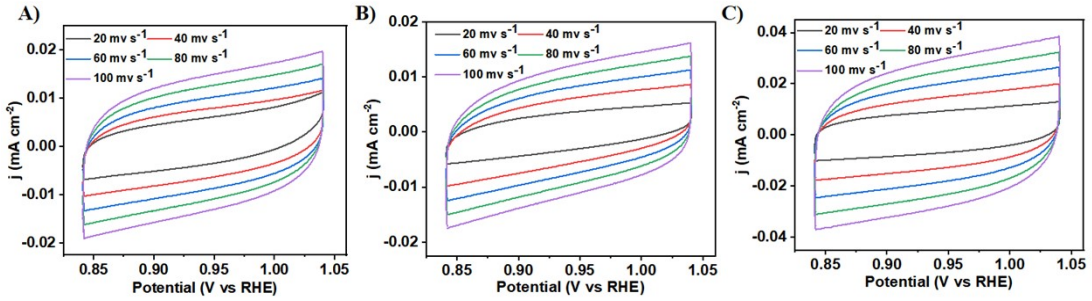

Figure S20. A) The CV of the $Ag_{20}Cu_{10}$@C; B) The CV of the Ag_8Cu_{12}@C; C) The CV of the $Ag_{17}Cu_{15}$@C.

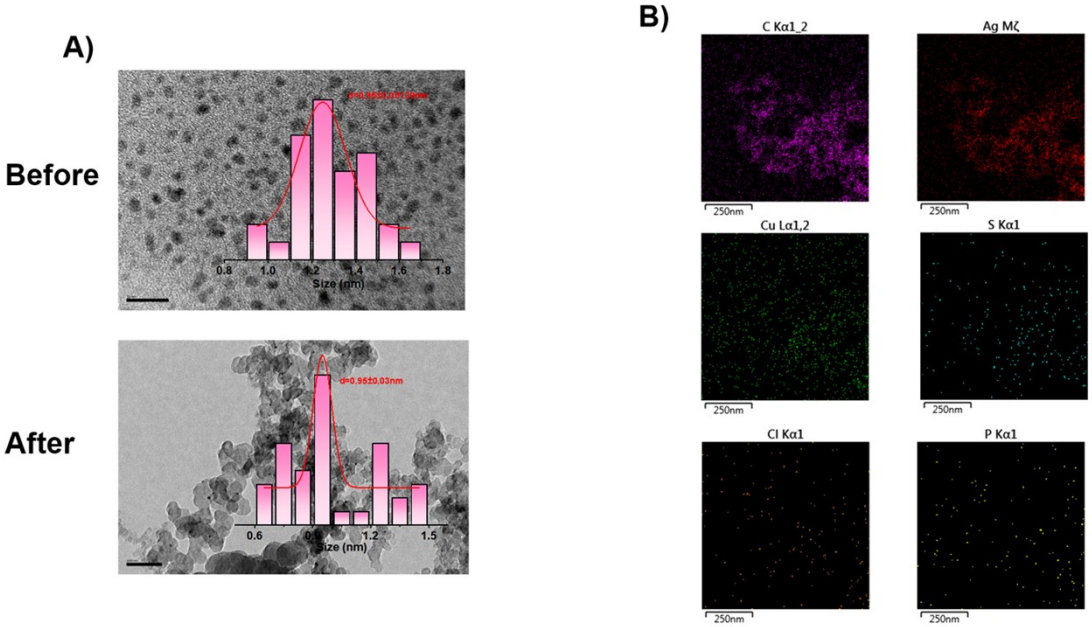

Figure S21. TEM of $Ag_{20}Cu_{10}$ and $Ag_{20}Cu_{10}$@C; B) EDS of $Ag_{20}Cu_{10}$@C.

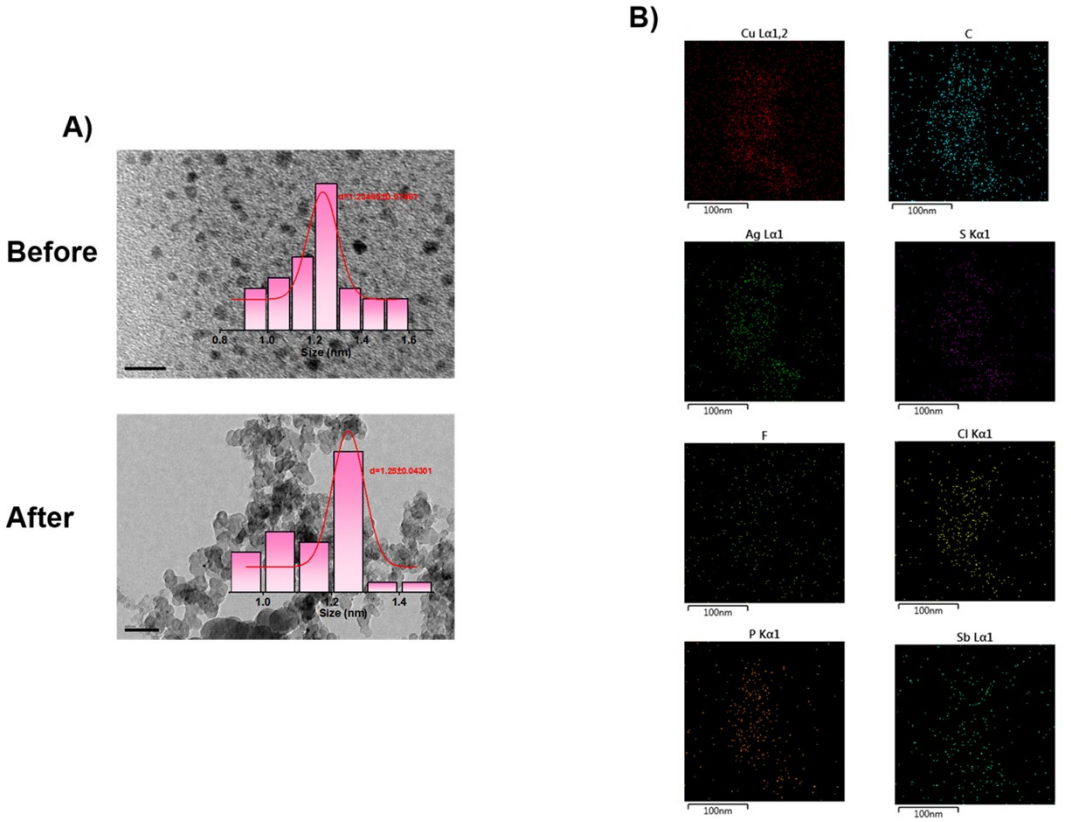

Figure S22. TEM of Ag_8Cu_{12} and Ag_8Cu_{12}@C; B) EDS of Ag_8Cu_{12}@C.

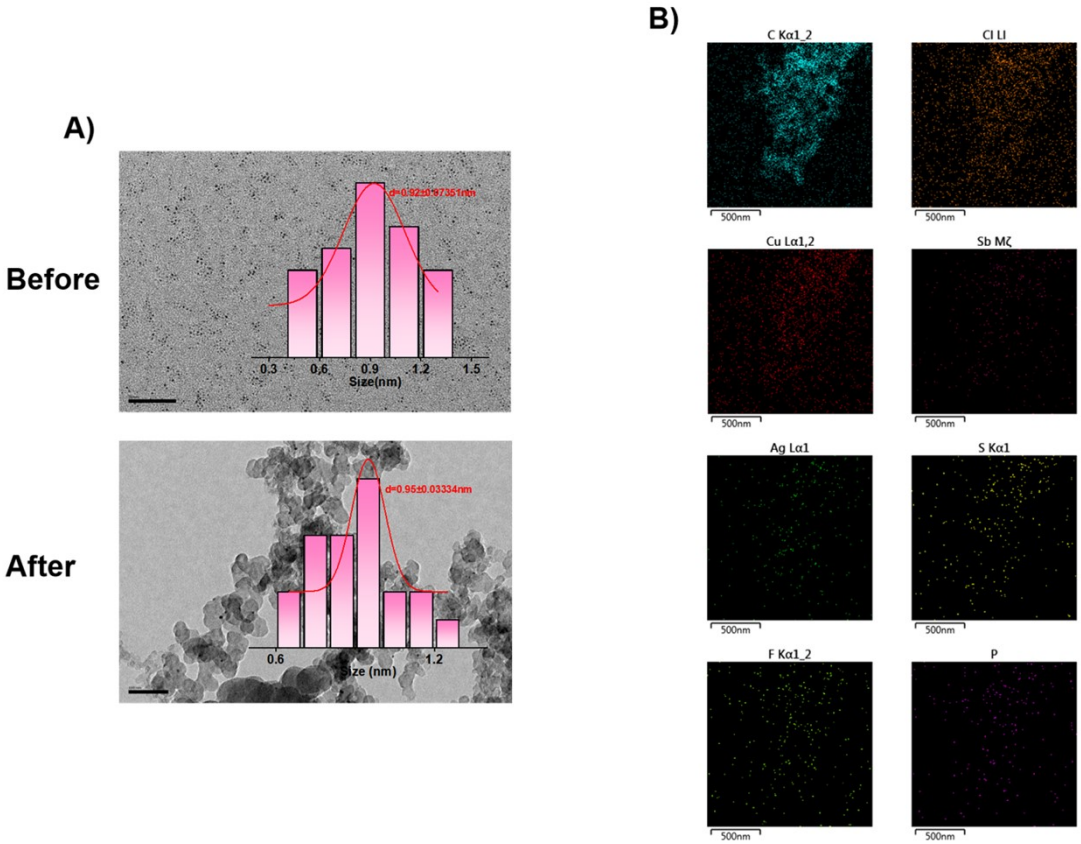

Figure S23. TEM of $Ag_{17}Cu_{15}$ and $Ag_{17}Cu_{15}$@C; B) EDS of $Ag_{17}Cu_{15}$@C.

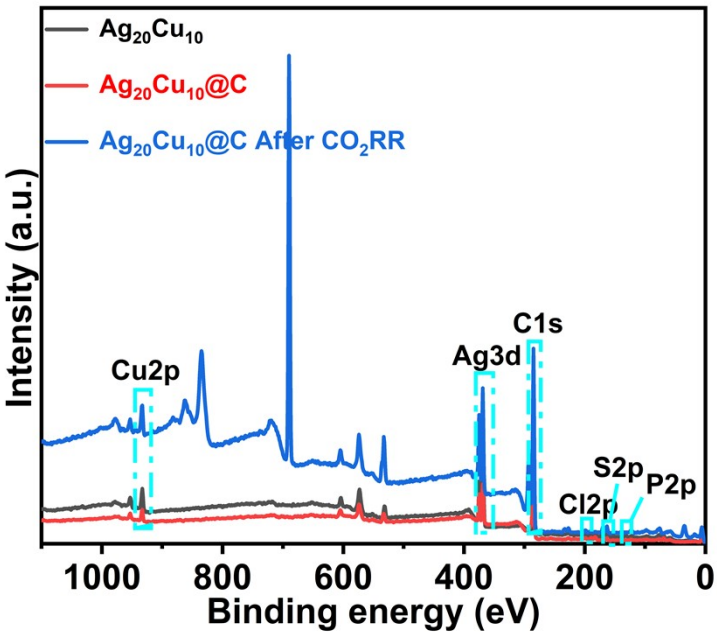

Figure S24. XPS spectra of pure clusters, catalysts and catalysts after catalysis of $Ag_{20}Cu_{10}$.

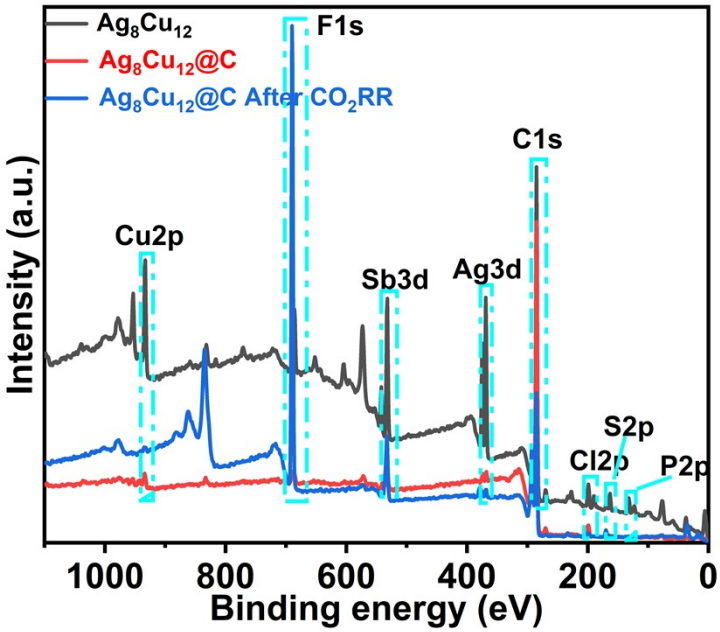

Figure S25. XPS spectra of pure clusters, catalysts and catalysts after catalysis of Ag_8Cu_{12}.

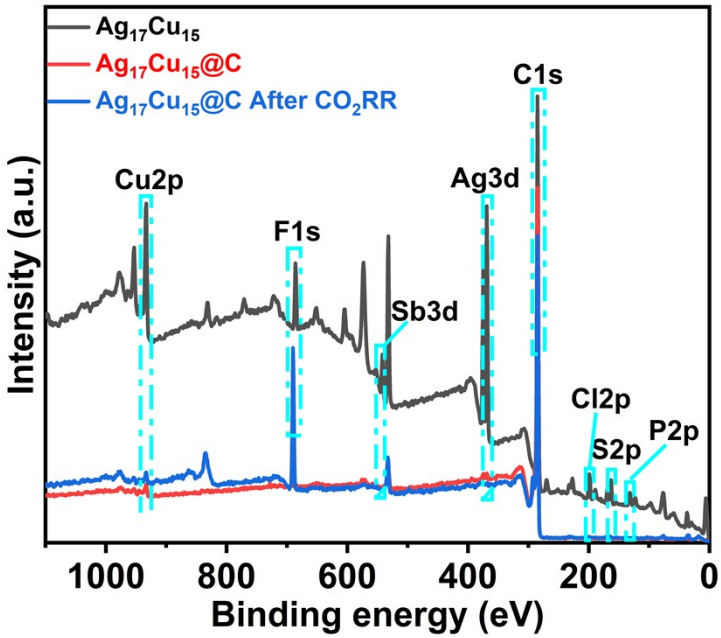

Figure S26. XPS spextra of pure clusters, catalysts and catalysts after catalysis of $\mathbf{Ag_{17}Cu_{15}}$.

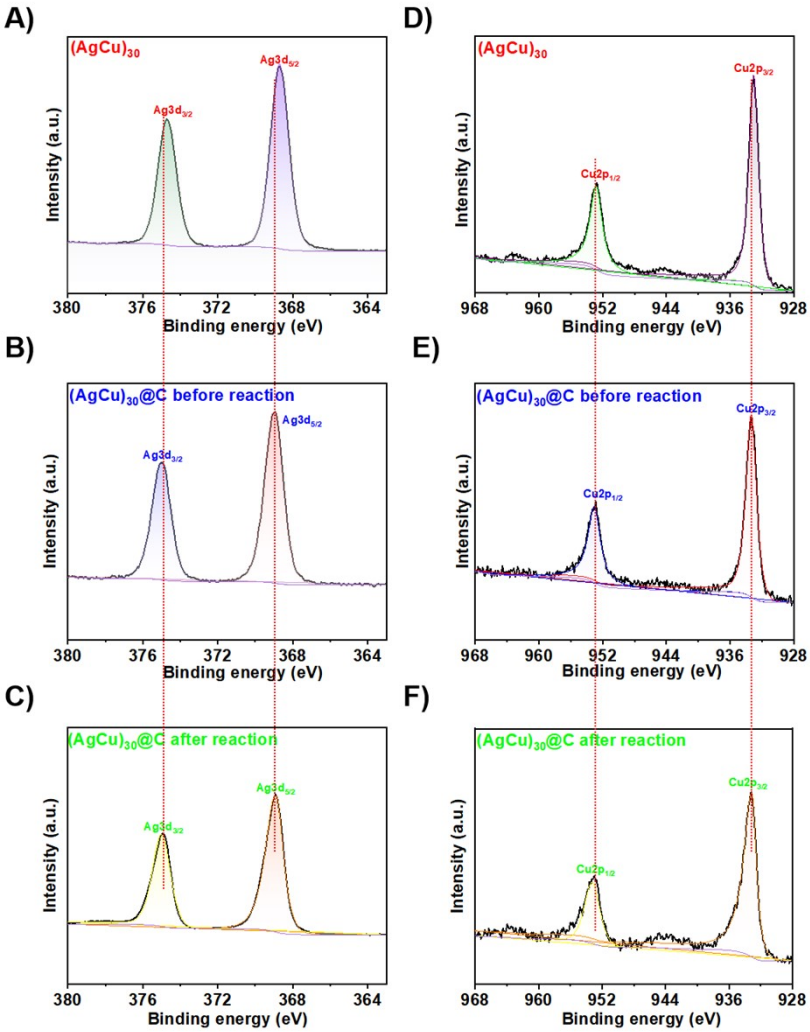

Figure S27. The XPS data of Ag and Cu for the $\mathbf{Ag_{20}Cu_{10}}$ catalysts.

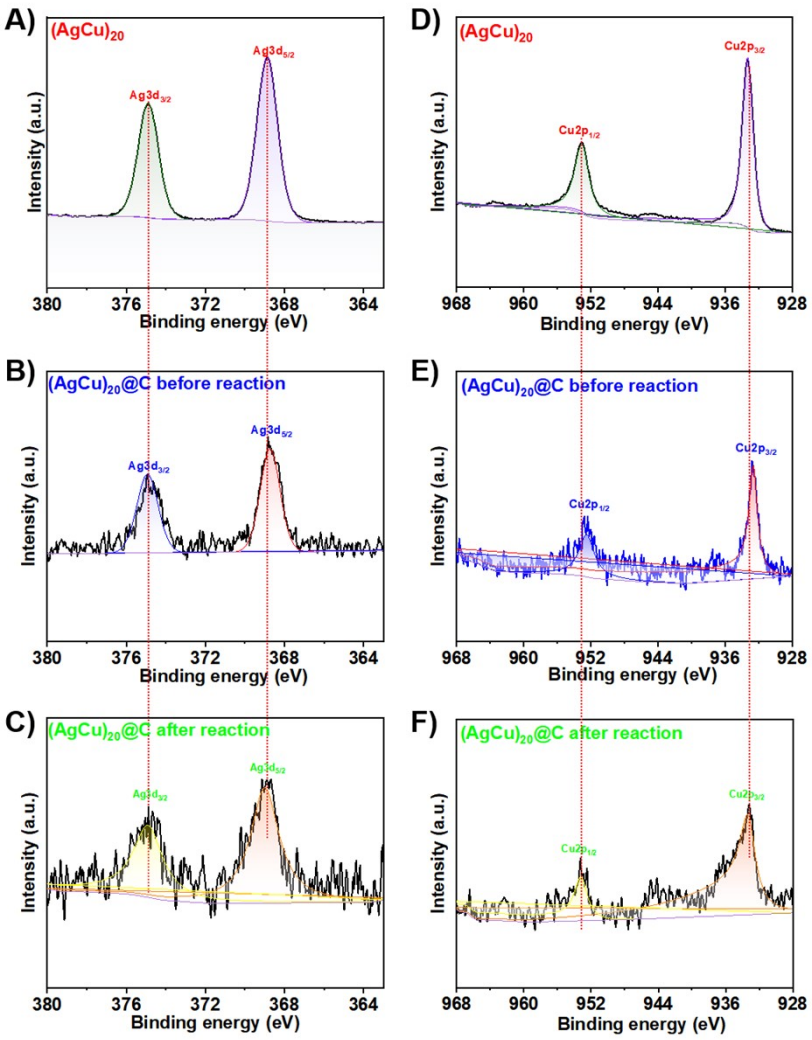

Figure S28. The XPS data of Ag and Cu for the $\mathbf{Ag_8Cu_{12}}$ catalysts.

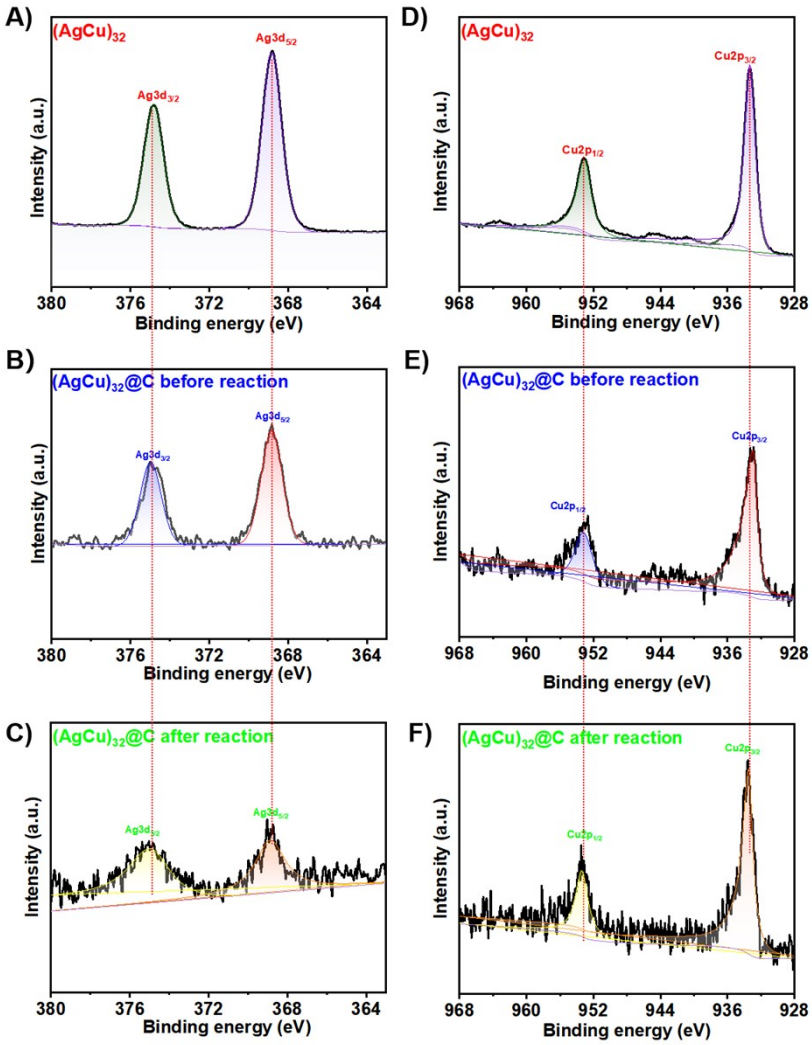

Figure S29. The XPS data of Ag and Cu for the $Ag_{17}Cu_{15}$ catalysts.

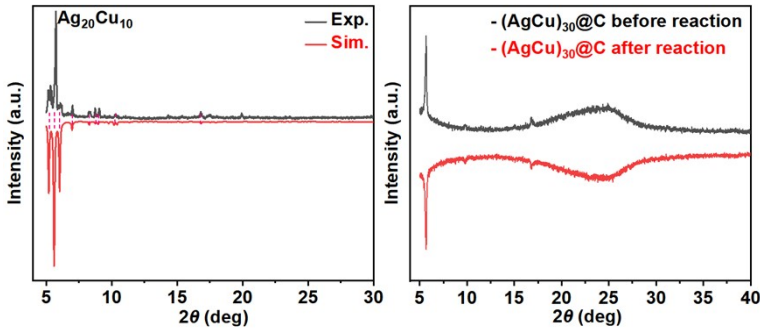

Figure S30. The PXRD of the $Ag_{20}Cu_{10}$ as well as $Ag_{20}Cu_{10}$@C before and after the electrocatalytic reaction

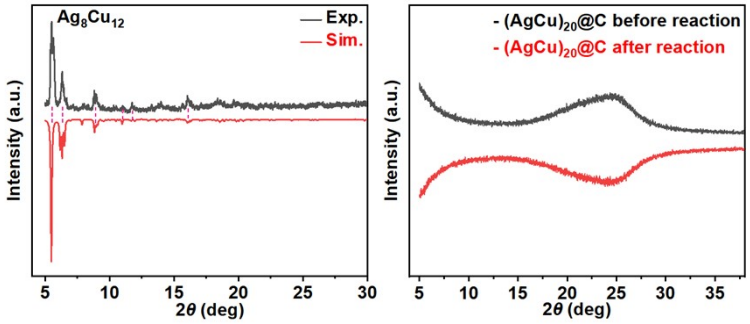

Figure S31. The PXRD of the Ag_8Cu_{12} clusters as well as Ag_8Cu_{12}@C before and after the electrocatalytic reaction.

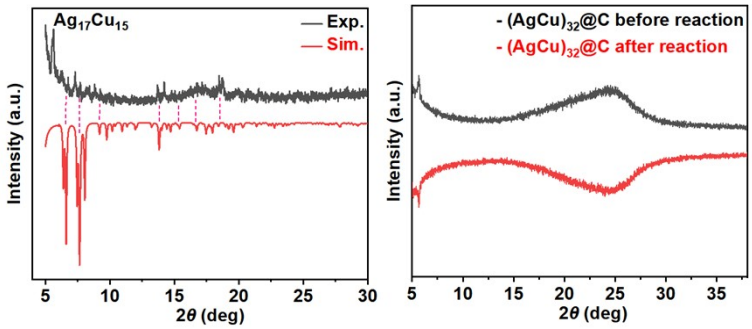

Figure S32. The PXRD of the $Ag_{17}Cu_{15}$ clusters as well as $Ag_{17}Cu_{15}$@C before and after the electrocatalytic reaction.

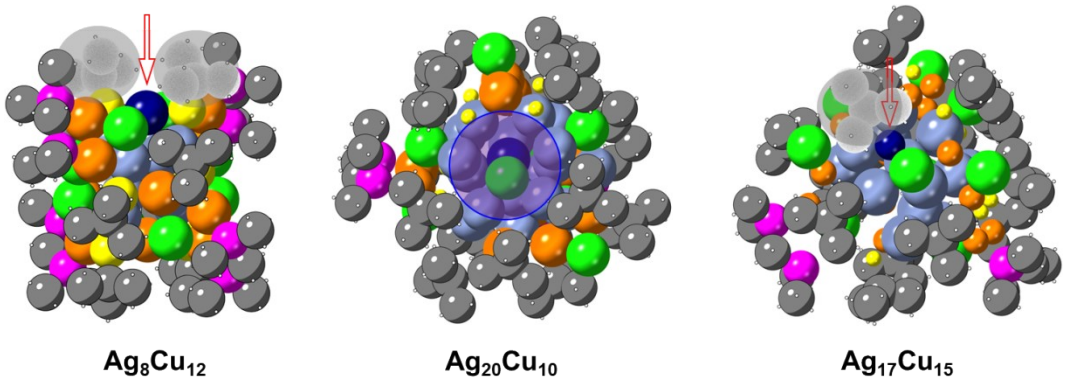

Figure S33. A comparison of the steric hindrance at CO_2 adsorption sites in three different Ag@Cu alloy clusters.

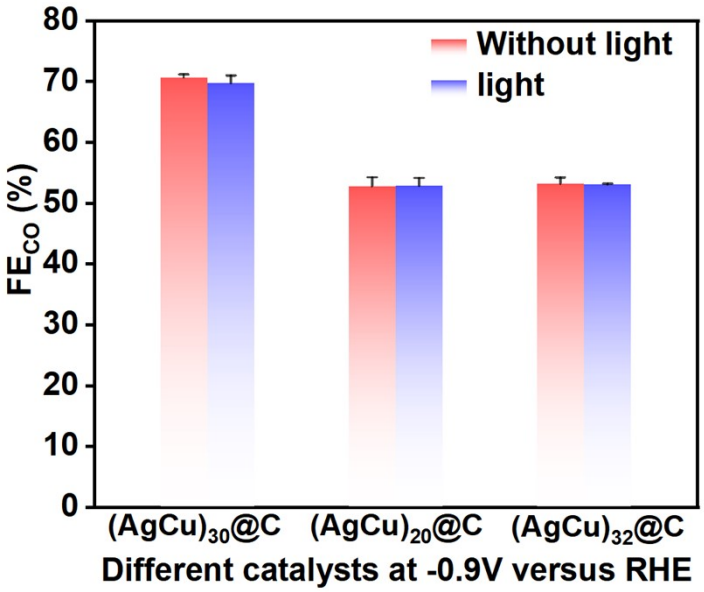

Figure S34. Faradaic efficiency of CO_2 for these three Ag-Cu alloy nanoclusters at -0.9 V vs. RHE, with and without additional illumination. Values are means, and error bars represent the standard deviation from several independent measurements (n ⩾3).

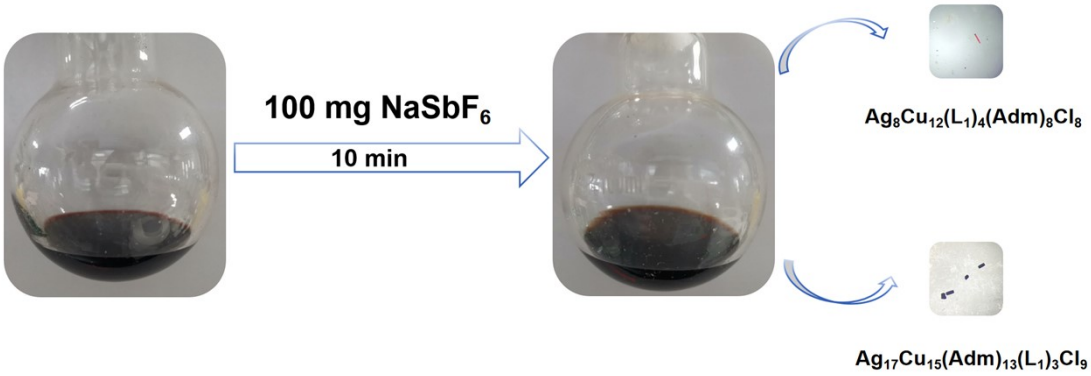

Figure S35. The synthesis of the $[Ag_8Cu_{12}(Dppm)_4(SAdm)_8Cl_8](SbF_6)_2$ and $[Ag_{17}Cu_{15}(Dppm)_3(SAdm)_{13}Cl_9](SbF_6)_2$ nanocluster. The transformation of $Ag_{20}Cu_{10}$ into Ag_8Cu_{12} and $Ag_{17}Cu_{15}$ upon introducing $NaSbF_6$ likely results from ion-induced structural rearrangement. SbF_6^- ions interact with the metal-ligand framework, destabilizing $A_{g20}Cu_{10}$ and facilitating the formation of new, thermodynamically or kinetically favored clusters (Ag_8Cu_{12} and $Ag_{17}Cu_{15}$). This process may involve ligand removal or replacement, metal atom redistribution, or changes in the oxidation states of Ag and Cu, influenced by the coordination preferences of SbF_6^-. And experimental results indicate that varying $NaSbF_6$ concentration, reaction temperature, solvent polarity, and reaction time does not yield a single product. Limited studies on $NaSbF_6$-induced transformations highlight the need for further investigation into its mechanism, offering new strategies to control cluster structures.

Table S1. Crystal data and structure refinement for $AgCu)_{30}$.

Identification code	$AgCu)_{30}$
Empirical formula	$C_{191}H_{256}Ag_{20}Cl_{10}Cu_{10}P_4S_{14}$
Formula weight	6271.96
Temperature/K	120(2)
Crystal system	monoclinic
Space group	$P2_1$
a/Å	21.403(2)
b/Å	20.1937(18)
c/Å	25.418(2)
α/°	90
β/°	94.635(7)
γ/°	90
Volume/Å^3	10949.9(17)
Z	2
ρ_{calc}g/cm^3	1.902
Radiation	CuKα (λ = 1.54186)
2θ range for data collection/°	11.206 to 139.512
Index ranges	$-25 \leq h \leq 25$, $-18 \leq k \leq 24$, $-30 \leq l \leq 26$
Reflections collected	55554
Independent reflections	27000 [R_{int} = 0.0288, R_{sigma} = 0.0241]
Data/restraints/parameters	27000/2895/2170
Goodness-of-fit on F^2	1.022
Final R indexes [I>=2σ (I)]	R_1 = 0.0551, wR_2 = 0.1491
Final R indexes [all data]	R_1 = 0.0578, wR_2 = 0.1524
Largest diff. peak/hole / e Å^{-3}	1.24/-1.44
Flack parameter	0.449(5)

Table S2. Crystal data and structure refinement for $AgCu)_{20}$.

Identification code	$AgCu)_{20}$
Empirical formula	$C_{193.6}H_{237.2}Ag_8Cl_{19.2}Cu_{12}F_{12}O_2P_8S_8Sb_2$
Formula weight	5878.04
Temperature/K	120(2)
Crystal system	orthorhombic
Space group	Pnna
a/Å	28.677(2)
b/Å	27.162(2)
c/Å	27.948(2)
α/°	90
β/°	90
γ/°	90
Volume/Å^3	21770(3)
Z	4
ρ_{calc}g/cm^3	1.793
Radiation	CuKα (λ = 1.54186)
2θ range for data collection/°	11.68 to 140.478
Index ranges	$-34 \leq h \leq 23$, $-24 \leq k \leq 32$, $-34 \leq l \leq 30$
Reflections collected	127801
Independent reflections	20348 [R_{int} = 0.0636, R_{sigma} = 0.0435]
Data/restraints/parameters	20348/664/1220
Goodness-of-fit on F^2	1.080
Final R indexes [I>=2σ (I)]	R_1 = 0.0700, wR_2 = 0.2052
Final R indexes [all data]	R_1 = 0.0858, wR_2 = 0.2196
Largest diff. peak/hole / e Å^{-3}	4.21/-1.31

Table S3. Crystal data and structure refinement for $AgCu)_{32}$.

Identification code	$AgCu)_{32}$
Empirical formula	$C_{205}H_{261}Ag_{17.11}Cl_9Cu_{14.89}F_{12.06}P_6S_{13}Sb_{2.01}$
Formula weight	6912.46
Temperature/K	120(2)
Crystal system	trigonal
Space group	R-3
a/Å	26.715(4)
b/Å	26.715(4)
c/Å	68.924(9)
α/°	90
β/°	90
γ/°	120
Volume/Å^3	42602(14)
Z	5.99994
ρ_{calc}g/cm^3	1.617
Radiation	CuKα (λ = 1.54186)
2θ range for data collection/°	7.656 to 129.986
Index ranges	$-31 \leq h \leq 23$, $-31 \leq k \leq 30$, $-73 \leq l \leq 80$
Reflections collected	76725
Independent reflections	15477 [R_{int} = 0.0977, R_{sigma} = 0.0955]
Data/restraints/parameters	15477/1127/820
Goodness-of-fit on F^2	1.233
Final R indexes [I>=2σ (I)]	R_1 = 0.1507, wR_2 = 0.3664
Final R indexes [all data]	R_1 = 0.1839, wR_2 = 0.3850
Largest diff. peak/hole / e Å^{-3}	4.30/-2.09

Table S4. Attribution of absorption peaks in the computed spectrum of Ag_8Cu_{12}.

Peak (nm)	Excited state (S_n)	Excited energy (eV)	*f*	Contribution for Peak*	Transition mode/contribution for S_n
551	1	2.14	0.0616	11.74%	H-1 → L 48.7%
					H → L 43.7%
	2	2.166	0.10596	24.14%	H → L 44.4%
					H-1 → L 42.0%
	3	2.25	0.01681	24.14%	H-2 → L 88.1%
	4	2.273	0.10177	28.39%	H → L+1 63.9%
					H-5 → L 12.0%
					H-1 → L+1 6.9%
					H-4 → L 6.8%
	5	2.324	0.05253	12.60%	H-3 → L 61.1%
					H-1 → L+1 22.7%
	6	2.337	0.03765	8.46%	H-4 → L 35.7%
					H-5 → L 25.6%
					H → L+1 13.2%
					H-3 → L 13.2%
	7	2.339	0.03401	7.56%	H-1 → L+1 60.1%
					H-3 → L 18.2%
					H → L+1 10.2%
382	50	3.206	0.01343	5.40%	H-26 → L 72.0%
					H-20 → L+1 7.2%
					H-22 → L 5.9%
	52	3.245	0.09616	40.60%	H → L+2 71.6%
					H-21 → L+1 6.1%
	54	3.277	0.0173	7.08%	H-23 → L+1 41.3%
					H-24 → L+1 28.6%
					H-25 → L+1 8.1%
					H-22 → L+1 7.3%
	55	3.3	0.02779	10.72%	H-24 → L+1 42.0%
					H-25 → L+1 29.7%
					H-23 → L+1 6.6%
324*	93	3.787	0.02604	7.33%	H-9 → L+2 31.7%, H-8 → L+2 11.9%, H-42 → L 9.9%, H-41 → L 6.7%, H-46 → L 6.1%, H-37 → L+1 5.8%, H-40 → L 5.6%
	95	3.802	0.02123	6.16%	H-38 → L+1 55.5%
	102	3.894	0.02519	6.48%	H-10 → L+2 33.9%, H-12 → L+2 9.8%, H-47 → L 6.1%, H-52 → L 6.1%

* refers to the contribution of transition mode $S_0 \rightarrow S_n$ to the absorption peak.

Table S5. Attribution of absorption peaks in the computed spectrum of $Ag_{20}Cu_{10}$.

Peak (nm)	Excited state (S_n)	Excited energy (eV)	*f*	Contribution for Peak*	Transition mode/contribution for S_n
486	15	2.46	0.0681	7.13%	H-3 → L+1 30.8%, H-2 → L+3 30.6%, H-2 → L+2 6.9%, H-3 → L+2 6.8%, H-1 → L+4 6.5%, H → L+4 5.3%
	17	2.484	0.12093	14.63%	H-5 → L 56.0%, H-2 → L 6.0%, H-4 → L+2 5.5%, H-4 → L+1 5.3%
	18	2.501	0.17217	22.10%	H-5 → L 29.1%, H-4 → L+1 10.6%, H-2 → L 9.6%, H-4 → L+2 6.8%
	19	2.522	0.10913	14.76%	H-4 → L+2 39.2%, H-4 → L+1 22.3%, H-6 → L 6.3%, H-2 → L 5.6%
	20	2.569	0.04485	6.16%	H-6 → L 64.5%, H-5 → L+1 7.4%
	29	2.71	0.0821	5.21%	H → L+4 15.3%, H-1 → L+4 11.3%, H-3 → L+3 8.9%, H-7 → L+1 7.3%, H-11 → L 6.5%
406	47	2.966	0.03588	5.49%	H-7 → L+3 25.9%, H-10 → L+2 10.3%, H-2 → L+4 9.6%, H-13 → L 7.5%, H-5 → L+3 5.1%
	48	2.97	0.04559	7.15%	H-2 → L+4 20.4%, H-14 → L 19.9%, H-6 → L+3 6.7%, H-7 → L+3 5.2%, H-10 → L+2 5.0%
	51	2.999	0.05034	8.92%	H-6 → L+3 15.5%, H-15 → L 13.2%, H-7 → L+3 10.3%, H-2 → L+4 8.6%, H-12 → L+1 6.1%, H-16 → L 5.7%, H-10 → L+2 5.5%
	57	3.068	0.03819	7.38%	H-12 → L+2 10.7%, H-13 → L+1 10.3%, H-15 → L+2 9.8%, H-15 → L+1 8.7%, H-20 → L 5.9%
357	107	3.439	0.05654	5.77%	H-19 → L+3 24.0%, H-30 → L 17.1%, H-21 → L+3 9.8%, H-20 → L+2 6.3%, H-17 → L+3 5.2%
	110	3.463	0.14526	15.30%	H-19 → L+3 10.4%, H-24 → L+1 9.8%, H-25 → L+1 8.8%, H-16 → L+3 7.2%, H → L+5 5.5%, H-30 → L 5.4%, H-1 → L+5 5.2%, H-20 → L+2 5.0%

* refers to the contribution of transition mode $S_0 \rightarrow S_n$ to the absorption peak.

Table S6. Attribution of absorption peaks in the computed spectrum of $Ag_{17}Cu_{15}$.

Peak (nm)	Excited state (S_n)	Excited energy (eV)	*f*	Contribution for Peak*	Transition mode/contribution for S_n
625	4	1.866	0.02307	6.93%	H-1 → L+1 28.3%, H-2 → L 17.7%, H-4 → L+1 15.0%, H → L 10.3%, H-1 → L 7.9%, H → L+2 5.0%
	5	1.878	0.02733	8.93%	H-2 → L+1 27.5%, H-2 → L 20.2%, H-3 → L 18.3%, H → L 14.2%
	6	1.888	0.03503	12.16%	H-1 → L+1 35.3%, H-2 → L 23.2%, H-3 → L 9.1%, H → L+1 7.6%, H-3 → L+1 5.3%
	8	1.986	0.05001	23.07%	H-4 → L 36.1%, H-3 → L+1 26.5%, H-1 → L+1 6.7%
	9	1.997	0.06928	31.80%	H-3 → L 27.9%, H-4 → L+1 27.8%, H → L 7.1%, H-3 → L+1 6.6%, H → L+1 6.1%
451	27	2.588	0.08123	5.41%	H-1 → L+3 22.5%, H → L+5 15.6%, H-8 → L+1 13.6%, H-2 → L+4 8.5%, H → L+2 6.7%, H → L+3 6.6%
	28	2.619	0.06645	5.59%	H-2 → L+3 24.3%, H-4 → L+3 21.7%, H-1 → L+4 18.5%, H-8 → L 13.0%
	30	2.635	0.05595	5.57%	H-10 → L 21.4%, H-2 → L+4 18.0%, H → L+4 8.0%, H-13 → L 7.5%, H-12 → L+1 5.3%
	33	2.662	0.05873	6.90%	H-4 → L+3 55.1%, H-1 → L+4 7.9%
	45	2.816	0.20137	26.10%	H → L+5 15.1%, H → L+2 6.5%, H-13 → L+1 5.8%, H-15 → L+1 5.8%
353	109	3.418	0.05569	5.37%	H-15 → L+2 19.8%, H-2 → L+6 8.9%, H-10 → L+4 7.3%, H-29 → L 7.0%, H-11 → L+3 5.6%
	120	3.481	0.05661	6.95%	H-4 → L+6 33.0%, H-32 → L 12.5%
	122	3.487	0.04112	5.10%	H-13 → L+3 25.8%, H-4 → L+6 11.7%, H-3 → L+6 8.7%, H-31 → L+1 7.1%, H-11 → L+3 6.3%

* refers to the contribution of transition mode $S_0 \rightarrow S_n$ to the absorption peak.

Table S7. Summary of Faradaic Efficiency Data for Electrocatalytic CO_2 Reduction.

AgCu)$_{30}$@C	$\overline{FE_{CO}}$	$\overline{FE_{H2}}$	**FE$_{total}$**
-0.7V	**0**	**0**	**0**
-0.8V	**54.85**	**41.03**	**95.88**
-0.9V	**70.80**	**26.09**	**96.17**
-1.0V	**58.74**	**37.06**	**95.80**
-1.1V	**54.09**	**44.05**	**98.14**
AgCu)$_{20}$@C	$\overline{FE_{CO}}$	$\overline{FE_{H2}}$	**FE$_{total}$**
-0.7V	**16.27**	**0**	**16.27**
-0.8V	**40.54**	**0**	**40.54**
-0.9V	**52.70**	**42.90**	**95.60**
-1.0V	**43.19**	**54.10**	**97.29**
-1.1V	**38.05**	**58.19**	**96.24**
AgCu)$_{32}$@C	$\overline{FE_{CO}}$	$\overline{FE_{H2}}$	**FE$_{total}$**
-0.7V	**14.22**	**0**	**14.22**
-0.8V	**34.49**	**65.12**	**99.61**
-0.9V	**55.1**	**43.51**	**98.61**
-1.0V	**59.83**	**39.03**	**98.86**
-1.1V	**41.21**	**58.86**	**100.07**